The International Journal of Advanced Manufacturing Technology (2021) 115:581–593
https://doi.org/10.1007/s00170-021-07166-4

ORIGINAL ARTICLE

Experimental investigation of the effects of super-elasticity on the machinability of NiTi alloys

Hao Yang[1] · Katsuhiko Sakai[2] · Hiroo Shizuka[2] · Yuji Kurebayashi[2] · Kunio Hayakawa[2] · Tetsuo Nagare[3]

Received: 8 February 2021 / Accepted: 26 April 2021 / Published online: 12 May 2021

Abstract
Machining of NiTi alloys is a challenging task owing to their inherent material properties and unique phase transformation-based behaviors. In this study, the effects of super-elasticity on the machinability of room-temperature austenitic NiTi alloy were investigated through turning experiments conducted at various cutting speeds under the non-preheating and preheating conditions. As a result, the workpiece exhibited an unavoidable super-elastic shape recovery and underwent a partial phase transformation because the temperature of the workpiece had not exceeded the martensite desist temperature (M_d) during machining under the non-preheating condition. The super-elastic recovery of the workpiece resulted in the deterioration of the machinability, through the decrease in the dimension accuracy, increase in the cutting resistance, and shortening of the tool life. The deterioration of the machinability caused by super-elasticity was intensified with the increase in the cutting speed. However, an excessively low cutting speed of 10 m/min induced severe built-up edge deposition on the machined surface. When the workpiece was preheated to a temperature above the M_d, the dimension accuracy was enhanced, the cutting resistance decreased and the tool life was prolonged owing to the elimination of the effects of the super-elasticity. Therefore, machining at moderate cutting speeds in the range of 25 to 50 m/min after preheating the workpiece to a temperature above the M_d can improves the machinability of room-temperature austenitic NiTi alloy.

Keywords NiTi alloy · Super-elasticity · Temperature · Machinability · Preheating

1 Introduction

NiTi alloys exhibit unique functional properties including the shape memory effect and super-elasticity based on the phase transformation between the martensite and austenite phases induced by variable temperature or stress conditions. Specifically, NiTi alloys enter the austenite phase when heated to the austenite finish temperature (A_f); above this temperature, forward phase transformation from the austenite to the stress-induced martensite phase occurs when the specimen is loaded beyond the elastic limit. Although a relatively large strain is generated during the forward phase transformation, NiTi alloys undergo a reverse phase transformation from the stress-induced martensite to austenite phase when unloaded; in addition, the strain is eliminated concomitantly with the reverse phase transformation. Therefore, austenitic NiTi alloys exhibit super-elasticity, owing to which, they can withstand and recover a large deformation without undergoing plastic deformations, unlike most metallic materials [1, 2]. In addition to the two aforementioned properties, NiTi alloys exhibit a high biocompatibility and corrosion resistance and are thus promising candidates for fabricating actuators [3] and biomedical devices including endodontic root canals [4], orthodontic wires [5], vascular stents [6], and surgical catheters [7]. To ensure the required shape adaptability for such products, a high-accuracy machining process provides fine surface finish that is generally employed after casting and plastic forming during the manufacturing of NiTi-based products.

However, undesirable machinability characteristics, such as high cutting resistance [8], high strain hardening [9], excessive burr formation [10], and severe tool wear [11] often limit the production efficiency and increase the production cost of

✉ Katsuhiko Sakai
sakai.katsuhiko@shizuoka.ac.jp

1 Graduate School of Science and Technology, Shizuoka University, Hamamatsu 432-8561, Japan

2 Department of Mechanical Engineering, Shizuoka University, Hamamatsu 432-8561, Japan

3 National Institute of Technology, Numazu College, Numazu 410-8501, Japan

NiTi-based products. In addition to the inherent material properties, the unique properties corresponding to the phase transformation likely also affect the machinability of NiTi alloys [12, 13]. Kuppuswamy et al. [14] reported an extensive recoverable deformation of the workpiece above the A_f in the micro-milling of NiTi alloys. Yang et al. [15] investigated the shape recovery phenomenon of the workpiece in orthogonal cutting of room-temperature austenitic NiTi alloy and reported that this phenomenon exhibited a dependence on the workpiece temperature, which could be controlled by changing the cutting speed. In addition, the workpiece temperature has been noted to be a key factor in the machining of NiTi alloys as it directly affects their phase transformation behavior [16]. Based on this understanding, Kaynak et al. [16–18] examined the machining performance of room-temperature martensitic $Ni_{49.9}Ti_{50.1}$ (at.%) alloy with relatively high phase transformation temperatures under cryogenic cooling and preheating conditions. The results indicated that cryogenic machining could effectively enhance the machining performance by preserving the workpiece in the martensite phase during machining; by contrast, preheating did not lead to any positive effects, except for an enhancement in the surface integrity. Nevertheless, Otsuka et al. [1], Chen et al. [19], Motemani et al. [20], and Benafan et al. [21] have proved that NiTi alloys do not undergo any phase transformation when heated to a temperature above the martensite desist temperature (M_d). Thus, when heated to a temperature above the M_d, NiTi alloys do not exhibit the super-elasticity, and hence, they will be deformed plastically after elastic deformation, similar to most metallic materials. Accordingly, preheating the workpiece beyond the M_d could also be a promising technique to effectively change the machining performance of this material. However, most of the existing studies on the preheating-based machining have not considered the M_d and super-elasticity. Consequently, more systematic studies on the relationship among the workpiece temperature, super-elasticity, and machinability must be performed to extensively understand the machining mechanism and improve the machinability of NiTi alloys.

Considering this aspect, this study was aimed at clarifying the effects of super-elasticity on the machinability of NiTi alloys and optimizing the cutting speeds and conditions in the machining of this material. Turning experiments were conducted on room-temperature austenitic NiTi alloy at various cutting speeds under the non-preheating and preheating conditions. The temperatures of the workpiece and chip were measured using a thermal camera during machining. To express the super-elastic deformation of the workpiece quantitively, the radius recovery of the workpiece was measured using a micrometer. The variation in the maximum height of the surface profile after machining was evaluated using a surface profiler for numerically presenting the surface topography and verifying the correctness of the measurement results of the radius recovery. The phase transformation behavior of the workpiece was analyzed using an X-ray diffraction (XRD) device to clarify the mechanism of the super-elastic recovery of the workpiece. Moreover, the cutting resistance and tool wear progression were examined to evaluate the effect of the super-elastic recovery of the workpiece on the machinability. The results of this study suggest an approach to improve the machinability of NiTi alloys, which can be beneficial for the manufacturing of NiTi-based products.

2 Experimental procedures

2.1 Workpiece material

The employed $Ni_{50.95}Ti_{49.05}$ (at.%) alloy was fabricated through vacuum induction melting followed by hot forming and hot rolling. The as-received workpiece was in the form of a round bar with a 50 mm diameter and 120 mm length. The phase transformation temperatures of the as-received workpiece were measured using differential scanning calorimetry (DSC), and the martensite start temperature (M_s), martensite finish temperature (M_f), austenite start temperature (A_s), and A_f values were determined to be − 23.6, − 41.2, − 17.9, and − 2.5 °C, respectively, as shown in Fig. 1. The M_d of this material was approximately 150 °C. Therefore, in the temperature range of − 2.5 to 150 °C, this material was expected to be in the austenite phase and exhibit super-elasticity.

2.2 Cutting tools, parameters, and conditions

Figure 2 shows the schematic of the experimental setup. Turning experiments were conducted on a OKUMA general-purpose lathe. MITSUBISHI TNMG160408 (ISO grade S10) cemented carbide inserts with a single-layer AlTiN coating were employed. The tool holder was a MITSUBISHI PTGNR2020K16 device. The cutting parameters and conditions are listed in Table 1. The change in the cutting speed V_c considerably affects the temperature and

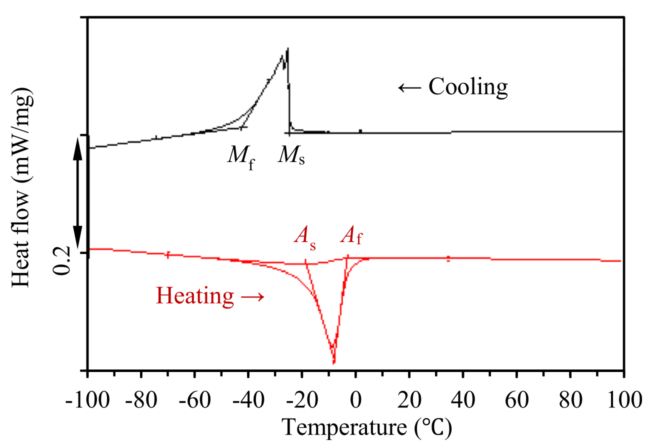

Fig. 1 DSC response of the workpiece material

Table 1 Cutting parameters and conditions

Cutting speed V_c (m/min)	10, 25, 50, 100
Cutting depth a_p (mm)	0.2
Feed rate f (mm/rev)	0.05
Conditions	Non-preheating, preheating
Lubrication	Dry

phase transformation of the NiTi alloy workpiece [13, 16]; hence, for this study, various cutting speeds in the range of 10 to 100 m/min were selected. A high cutting depth or feed rate significantly accelerates the tool wear rate and shortens the tool life [13]. Accordingly, to ensure an ideal tool life for better comparing this parameter under different cutting conditions, the cutting depth a_p and feed rate f were selected as 0.2 mm and 0.05 mm/rev, respectively. Machining under the non-preheating condition was conducted at room temperature (20 °C) without using any lubricant. Under the preheating condition, the workpiece installed in the chuck was preheated using a commercially available butane gas torch burner. To ensure that the temperature of the workpiece was maintained above the M_d at the beginning of machining without an excessive oxide layer being generated, the preheating temperature was set as 175 °C. The temperature of the workpiece was verified using a FLIR T450sc thermal camera. Figure 3 shows a sample thermal image of the workpiece after preheating. The turning experiments were initiated immediately after the temperature of the workpiece had reached the target temperature.

With reference to a previous study [22], an industrial electric heating plate with a maximum temperature of 300 °C and a K-type thermocouple were used to determine the emissivity of the workpiece material. A 1-mm-thick disk-shaped sample of the NiTi alloy with a well-machined end face was heated to several different temperatures using the heating plate. The thermal camera was used to calibrate the emissivity according to the temperature measured using the thermocouple. The emissivity for the machined surface of this material was determined to be 0.21. This result is consistent with those of previous studies [22, 23].

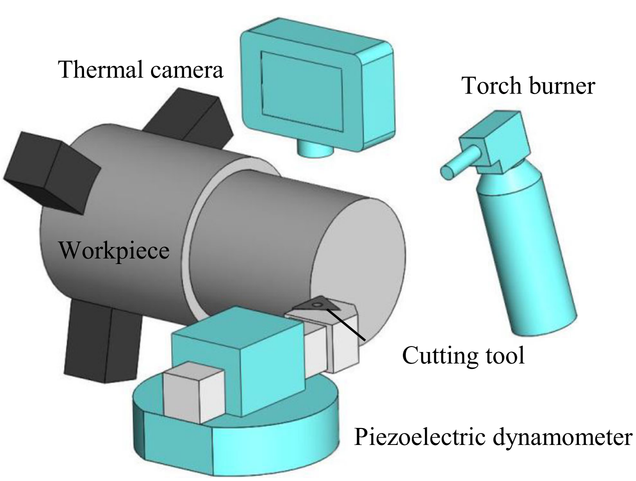

Fig. 2 Schematic of the experimental setup

2.3 Measurements

As shown in Fig. 4a and b, the temperature of the workpiece and chip were measured separately during machining under the non-preheating condition, considering two measurement ranges (20–200 °C for the workpiece and 200–1200 °C for the chip) to enable the colors in the thermal images to be distinguished more easily and to enhance the measurement accuracy. Under the preheating condition, the temperature of the workpiece exceeded 200 °C during machining, as shown in Fig. 4c. Therefore, the temperatures of the workpiece and chip were measured considering the same temperature range (200–1200 °C) under this condition. Thermal images with high clarity were used, and the measurement areas for the workpiece and chip were set close to the tool tip. For each measurement, 10 points in the measurement area were selected, and the temperatures at these points were determined using an analysis software (FLIR Tools); the average values for the 10 points were calculated as the results.

The radius recovery of the workpiece, r_R, was calculated using the following equation:

$$r_R = a_p - \frac{\left(d - d'\right)}{2}, \quad (1)$$

where d and d' denote the workpiece diameter before and after machining, respectively; a_p is the constant cutting depth of 0.2 mm. The d and d' were measured using a digital micrometer with a resolution of 1 μm. The d' values were measured 10 times at each cutting speed under both the non-preheating and preheating conditions. Considering that this measurement could be affected by the surface topography, the machined surface was observed using a digital camera, and the maximum height of the machined surface profile Rz was measured along the axial direction using a Mitutoyo SJ-210 stylus surface profiler.

The phase state of the workpiece was measured using the XRD technique in the as-received condition and after machining at the different cutting speeds under both the non-preheating and preheating conditions. In the as-received condition, the measurement sample was cut from the workpiece through wire electric discharge machining (WEDM). The measured surface was polished with a series of abrasive papers up to 1200 grit and ion-milled to remove the machining-induced layer generated during WEDM. In addition, after machining, samples were cut from the workpiece through WEDM, and XRD measurements were performed directly

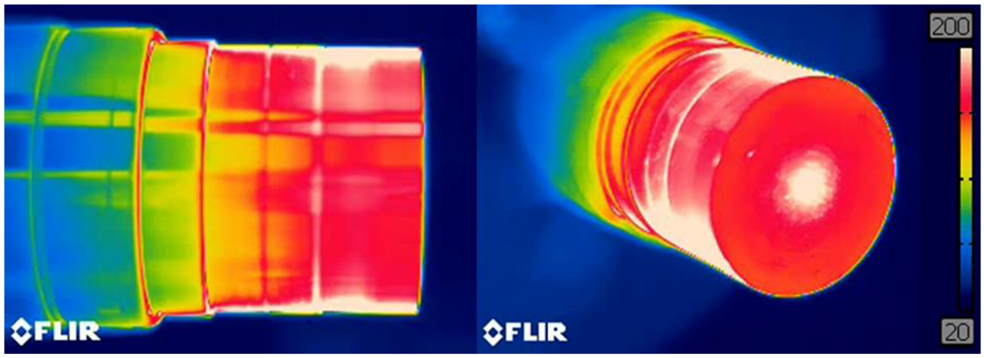

Fig. 3 Sample thermal image of the workpiece after preheating

on the machined surface. A Rigaku RINT-UltimaII XRD device with CuKα radiation was used for the measurement. The voltage and current of the X-ray tube were 40 kV and 40 mA, respectively. The diffraction angle 2θ range was set to 30–50°. The sampling interval and scanning speed were selected as 0.02° and 1°/min, respectively.

The cutting resistance values, including the main cutting force, radial force, and feed force, were measured using a KISTLER 9272 piezoelectric dynamometer. Moreover, the measurement of the average flank wear VB_a and observation of the tool wear morphology were realized using a HIROX KH-7700 digital microscope. According to ISO 3685:1993 [24], the tool wear test was continued until VB_a exceeded 0.3 mm or catastrophic failure at the cutting edge occurred. Because the temperature of the workpiece decreased after the measurement of VB_a, the workpiece was preheated repeatedly to the target temperature after each measurement under the preheating condition.

3 Results and discussion

3.1 Temperatures of the workpiece and chip during machining

The temperature of the workpiece during machining was considered to determine whether the temperature prerequisite for the phase transformation of the NiTi alloy had been satisfied. Figure 5 shows the temperature of the workpiece and chip measured during machining under both the non-preheating and preheating conditions. When the cutting speed increased from 10 to 100 m/min, the temperature of the chip and

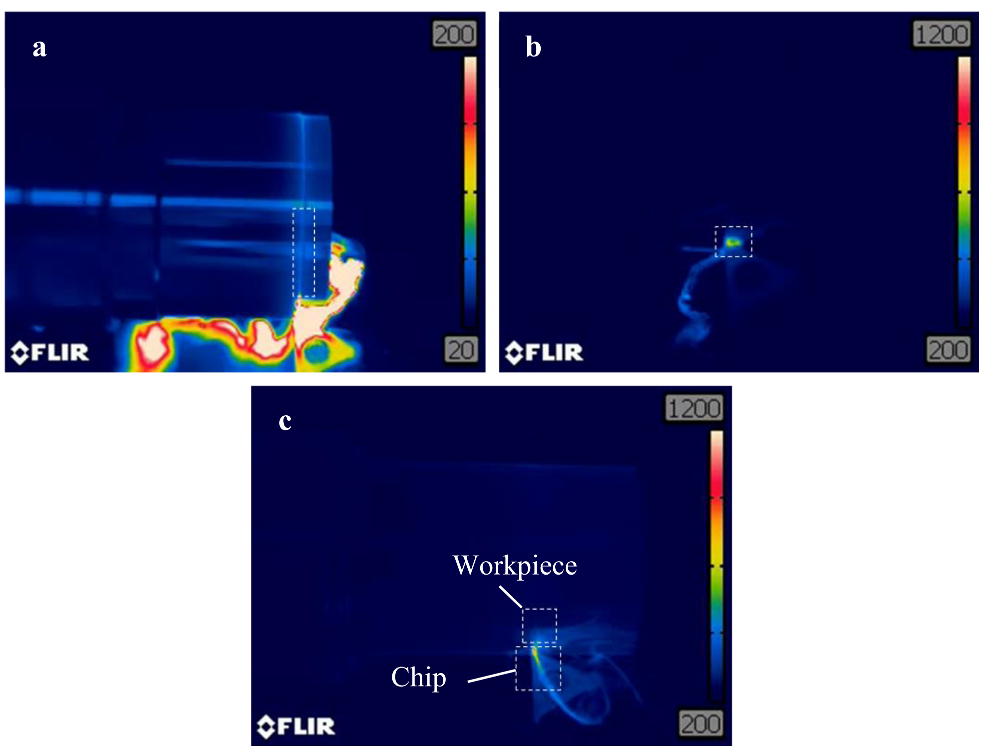

Fig. 4 Thermal images during machining at V_c = 100 m/min: **a** workpiece; **b** chip under non-preheating condition; **c** workpiece and chip under preheating condition

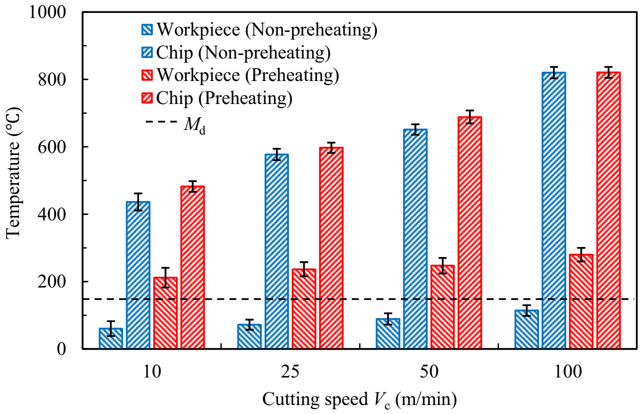

Fig. 5 Variation in temperatures of workpiece and chip

workpiece under the non-preheating condition increased from 436.4 to 820 °C and from 60.5 to 114.1 °C, respectively. Under the preheating condition, the two temperatures increased from 482.3 to 820.9 °C and from 211.8 to 280 °C, respectively. Although the temperatures of both the workpiece and chip increased with the increase in the cutting speed, the temperature of the chip was considerably higher than that of the workpiece for all the cutting speeds. Despite the fact that the absolute results of the temperature measurements were different owing to the different cutting parameters, the large temperature difference between the workpiece and chip during machining of NiTi alloys has been reported in previous studies as well [13, 15, 16]. Such a temperature distribution is generally observed in machining of metallic materials; therefore, this characteristic is not considered to be significantly affected by the unique phase transformation-based properties of NiTi alloys.

Moreover, the results illustrated that the temperature of the workpiece did not exceed the M_d at any of the considered cutting speeds during machining under the non-preheating condition, thereby indicating that the workpiece could deform super-elastically by undergoing the forward and reverse phase transformations. Therefore, it was deemed necessary to preheat the workpiece artificially to inhibit the phase transformation and eliminate the effect of the super-elasticity. The results also illustrated that the temperature of the workpiece during machining under the preheating condition exceeded the M_d at the considered cutting speeds; hence, the effect of super-elasticity was expected to be effectively eliminated under this condition. In general, the M_d values of NiTi alloys vary with the phase transformation temperatures, which are mainly affected by the Ni content [25] and type of heat treatment [26]. Therefore, room-temperature martensitic NiTi alloy with higher phase transformation temperatures has a higher M_d than room-temperature austenitic NiTi alloy does. In this context, although room-temperature martensitic $Ni_{49.9}Ti_{50.1}$ (at.%) workpieces have been heated to 175 °C in previous studies [16–18], the workpiece temperature likely did not exceed the M_d for the NiTi alloys adopted in those studies.

3.2 Super-elastic recovery and phase transformation behavior of the workpiece

The shape recovery of the workpiece can be considered to be a representation of the super-elastic deformation. To express the super-elastic deformation, the radius recovery of the workpiece r_R was calculated using Eq. (1), and the results are shown in Fig. 6. The workpiece exhibited a larger recovery under the non-preheating condition than that under the preheating condition. Under the non-preheating condition, r_R increased from 6.3 to 8.1 μm with the increase in the cutting speed from 25 to 100 m/min. By contrast, under the preheating condition, no evident variation in r_R occurred in the cutting speed range of 25 to 100 m/min. Nevertheless, the maximum r_R was observed at V_c = 10 m/min under both the non-preheating and preheating conditions.

Considering that the machined surface is generally uneven because of machining marks, the topography of the machined surface must be evaluated to verify the correctness of the results obtained using the micrometer. To avoid the influence of the tool wear on the results, the observations and measurements were conducted after relatively short machining experiments with new cutting tools. Figure 7 shows the optical images of the machined surface at different cutting speeds under both the conditions, obtained using a digital camera. A large amount of built-up edge (BUE) was deposited on the machined surface at V_c = 10 m/min under the non-preheating condition. Under the preheating condition, although the deposition of the BUE was notably reduced, a certain amount remained at V_c = 10 m/min. Thus, the machined surface was excessively rough at V_c = 10 m/min, even though the cutting tool was far from its life limit. The BUE deposition was effectively reduced with the increase in the cutting speed to 25 m/min or higher under both the conditions, as shown in Fig. 7.

To present the surface topography numerically, the maximum height of the machined surface profile *Rz* was measured, and the results are shown in Fig. 8. The *Rz* measured after machining at V_c = 10 m/min under the non-preheating and

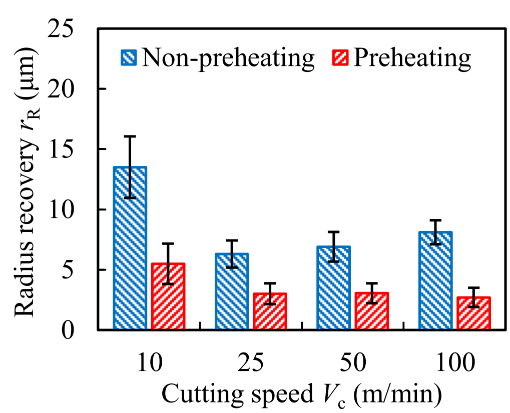

Fig. 6 Variation in radius recovery of workpiece

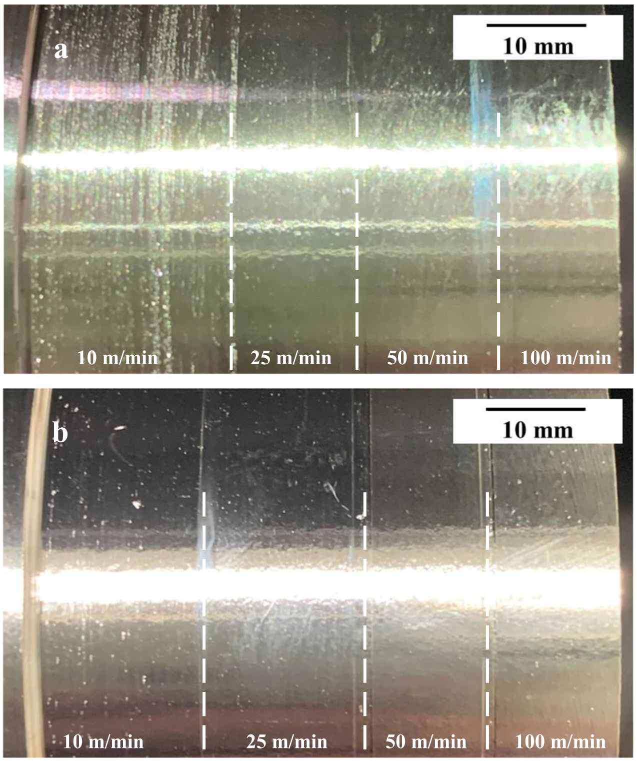

Fig. 7 Optical image of machined surface under **a** non-preheating condition and **b** preheating condition

preheating conditions were 13.5 μm and 5.5 μm, respectively. The values were considerably higher than that measured before machining (3.421 μm). Because the measurement faces of the anvil and spindle of the micrometer were likely only in contact with the high positions of the machined surface, the large values of r_R at V_c = 10 m/min shown in Fig. 6 could be attributed to the increase in Rz caused by the deposition of BUE. Thus, although the workpiece was expected to undergo a certain super-elastic recovery at this cutting speed, the value of r_R could not be accurately measured. At cutting speeds other than 10 m/min, Rz did not vary significantly after

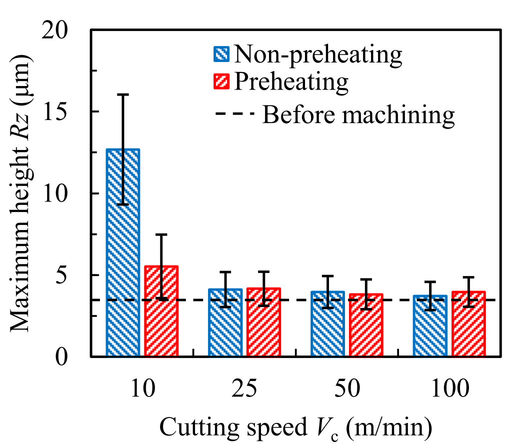

Fig. 8 Variation in maximum height of surface profile before and after machining

machining, as shown in Fig. 6. Thus, the measured results of r_R at the cutting speeds shown in Fig. 5 were considered reliable.

In general, metallic materials usually undergo elastic recovery during the machining process; however, because the recovery value is fairly small, generally less than 1 μm, this phenomenon is investigated primarily in precision or ultra-precision machining [27–29]. Notably, the super-elastic recovery of the NiTi workpiece was pronounced even during the conventional machining performed in this study. In addition to turning, the super-elastic recovery of the workpiece has also been observed in micro-milling [14] and orthogonal cutting [15] of NiTi alloys. A larger shape recovery of the workpiece is expected to lead to additional engineering tolerance, corresponding to a lower dimensional accuracy. This decrease in the dimension accuracy is unavoidable during machining under the non-preheating condition and is in fact further intensified with an increase in the cutting speed. Furthermore, the super-elastic recovery likely increases the contact area between the flank face of the tool and workpiece, thereby affecting the cutting resistance and tool wear; this aspect is discussed in Sections 3.3 and 3.4. Preheating the workpiece beyond the M_d can effectively enhance the dimension accuracy. Moreover, the setting with V_c = 10 m/min is not appropriate for machining NiTi alloys, because the corresponding severe BUE deposition degrades the surface finish. This finding is in accord with those of previous studies on the machining of NiTi alloys, in which BUE debris attached on the machined surface were observed at relatively low cutting speeds [16, 30, 31].

To clarify the variation trend of the super-elastic recovery of the workpiece under different cutting speeds and conditions, the phase transformation of the workpiece, which can be regarded as the mechanism of the super-elasticity, was analyzed through XRD measurements. Figure 9 shows the comparison of the XRD patterns of the as-received samples and machined samples at V_c = 25, 50, and 100 m/min under the non-preheating and preheating conditions. Because the severe deposition of BUE on the machined surface at V_c = 10 m/min also affected the XRD measurement, an accurate analysis could not be performed for this cutting speed. The sample in the as-received condition exhibited a high-intensity diffraction peak at 2θ = 42.38°, which corresponds to the austenite phase. This result illustrates that the as-received workpiece was completely in the austenite phase. After machining under the non-preheating condition, the intensity of the austenite peak considerably decreased. Moreover, the intensity exhibited an increasing trend with the increase in the cutting speed. In addition to the variation in the intensity, peak broadening and peak shifting occurred at all the cutting speeds. Moreover, diffraction peaks corresponding to the martensite phase were also observed, as shown in Fig. 9. In contrast to that of the austenite peak, the intensity of the

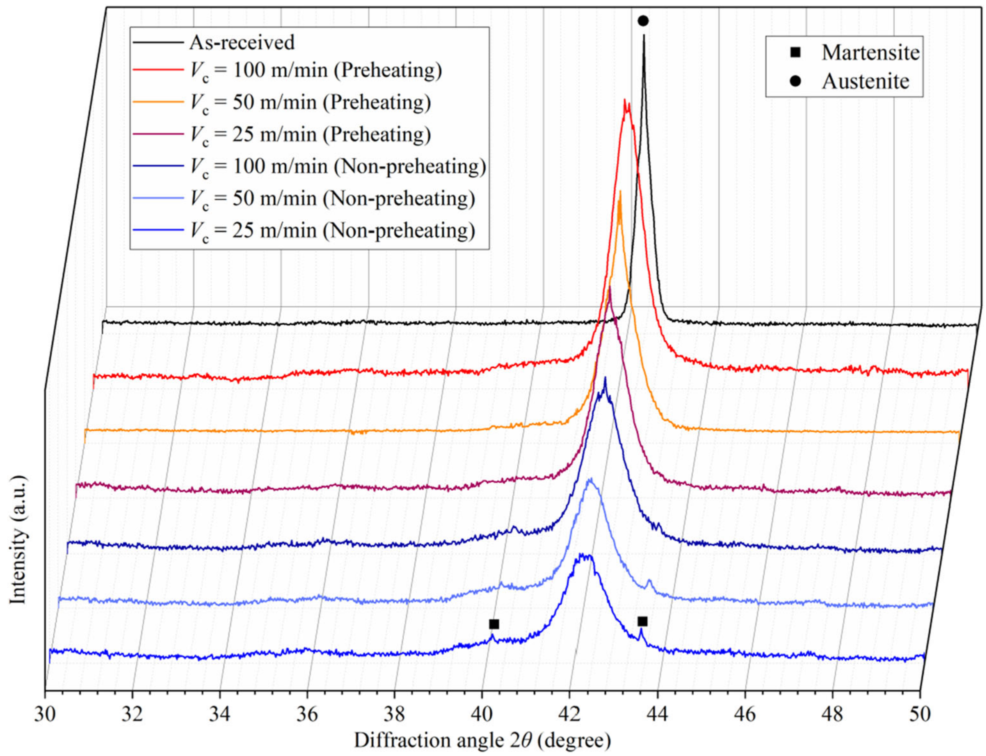

Fig. 9 XRD patterns of as-received and machined samples

martensite peak decreased slightly with the increase in the cutting speed.

As in the case of machining under the non-preheating condition, after machining under the preheating condition, the intensity of the diffraction peak of the austenite phase decreased, and peak broadening and peak shifting occurred. Nevertheless, in contrast to the non-preheating case, no pronounced martensite peak was observed after preheating-based machining.

Because the temperature of the workpiece did not exceed the M_d during machining under the non-preheating condition, as shown in Fig. 5, the austenite on the surface and subsurface of the workpiece near the tool tip likely underwent the forward phase transformation to martensite owing to the mechanical load. However, Otsuka et al. [1, 32] demonstrated that the reverse phase transformation of NiTi alloys will be suppressed by the high-density dislocation caused by plastic deformation. The density of dislocation generally increases in the machining-induced layer after the machining of metallic materials. Therefore, only part of the martensite on the surface and subsurface of the workpiece underwent the reverse phase transformation to austenite after the mechanical load was removed due to the suppression caused by the increase in the density of dislocation. The part that could not undergo the reverse phase transformation remained in the martensite phase. Thus, the volume of austenite and martensite decreased and increased in this process, respectively. Consequently, the austenite peak intensity decreased, and martensite peaks appeared after machining under the non-preheating condition, as shown in Fig. 9. Based on XRD analysis, Kaynak et al. [30, 33] and Zhao et al. [31] have also reported that the workpiece undergoes both the forward and reverse phase transformations during machining of room-temperature austenitic NiTi alloys. Moreover, the broadening and shifting of the austenite peak, which have also been reported in other studies on machining [18, 30, 31, 33] and cold working [34, 35] of NiTi alloys, can be attributed to the plastic deformation. Therefore, the substantial shape recovery of the workpiece during machining under the non-preheating condition, as shown in Fig. 6, is considered to be induced by this partial reverse phase transformation. Furthermore, according to Fig. 5, the temperature of the workpiece increased with the increase in the cutting speed. The higher temperature caused by a higher cutting speed likely alleviated the increase in the density of dislocation [30]. Thus, during machining at a higher cutting speed, a higher volume of martensite could undergo the reverse phase transformation to austenite, leading to greater super-elastic recovery. Consequently, with the increase in the cutting speed, the intensity of the martensite peak decreased, as shown in Fig. 9, and the radius recovery of the workpiece increased, as shown in Fig. 6.

The XRD patterns of the machined samples under the preheating condition mechanistically illustrate that the material on the surface and subsurface of the workpiece did not undergo any phase transformation during machining under the preheating condition. Consequently, the shape recovery of the workpiece was significantly smaller than that under the non-preheating condition at any cutting speed, as shown in Fig. 6.

Moreover, the results support a previously reported finding that the preheating-based machining can enhance the surface integrity of the NiTi alloy by preserving the initial phase state of the workpiece [18]. Furthermore, because no evident diffraction peak of oxide was observed after machining under the preheating condition, as shown in Fig. 9, the preheating temperature selected in this study was considered appropriate.

3.3 Cutting resistance

The aforementioned results verify the occurrence of the super-elastic recovery of the workpiece during machining under the non-preheating condition and the inhibition of the phase transformation through the preheating. In addition to the dimension accuracy, the cutting resistance, as another manifestation of the super-elastic recovery, was measured. Figure 10 shows the variation in the main cutting force, radial force, and feed force during machining at $V_c = 25$, 50, and 100 m/min under both the conditions. With the increase in the cutting speed, the main cutting force increased slightly under the non-preheating condition and decreased under the preheating condition. The radial force exhibited an increasing trend with the increase in the cutting speed under the non-preheating condition. Specifically, the radial force increased notably when the cutting speed increased from 50 to 100 m/min. At $V_c = 100$ m/min, the radial force exhibited the maximum value and emerged as the largest component of the cutting resistance (even larger than the main cutting force). Nevertheless, no evident variation in the radial force was observed at any of the considered cutting speeds under the preheating condition. The variation trend of the feed force was similar to that of the radial force. However, compared with those under the non-preheating condition, all the cutting resistance components, especially the radial force, decreased at the considered cutting speeds under the preheating condition. In particular, at V_c = 100 m/min, the radial force decreased by nearly 40% from 123.8 to 74.2 N.

In general, the main cutting force decreases with the increase in the cutting speed owing to thermal softening and a reduction in the friction coefficient between the tool and chip. As shown in Fig. 5, an increase in the cutting speed led to an increase in both the workpiece and chip temperatures. However, the results of this study indicate the abnormal variation in the cutting resistance, i.e., it increased with the increase in the cutting speed under the non-preheating conditions. In addition to this study, Weinert et al. [11] found that the main cutting forces increase significantly during turning under the non-preheating condition when the cutting speed exceeds 140 m/min. Moreover, Kaynak et al. [16] reported that the main cutting force increases with the increase in the cutting speed from 25 to 100 m/min. Nemat-Nasser et al. [36] and Adharapurapu et al. [37] reported that when the temperature is less than the M_d, the critical stress (determined by a strain offset of 0.2%) of room-temperature austenitic NiTi alloys, which is positively related to the strength of this material, increases with the increase in the temperature at a high strain rate of 1400/s and 1200/s. Therefore, higher cutting

Fig. 10 Variation in cutting resistance: **a** main cutting force, **b** radial force, and **c** feed force

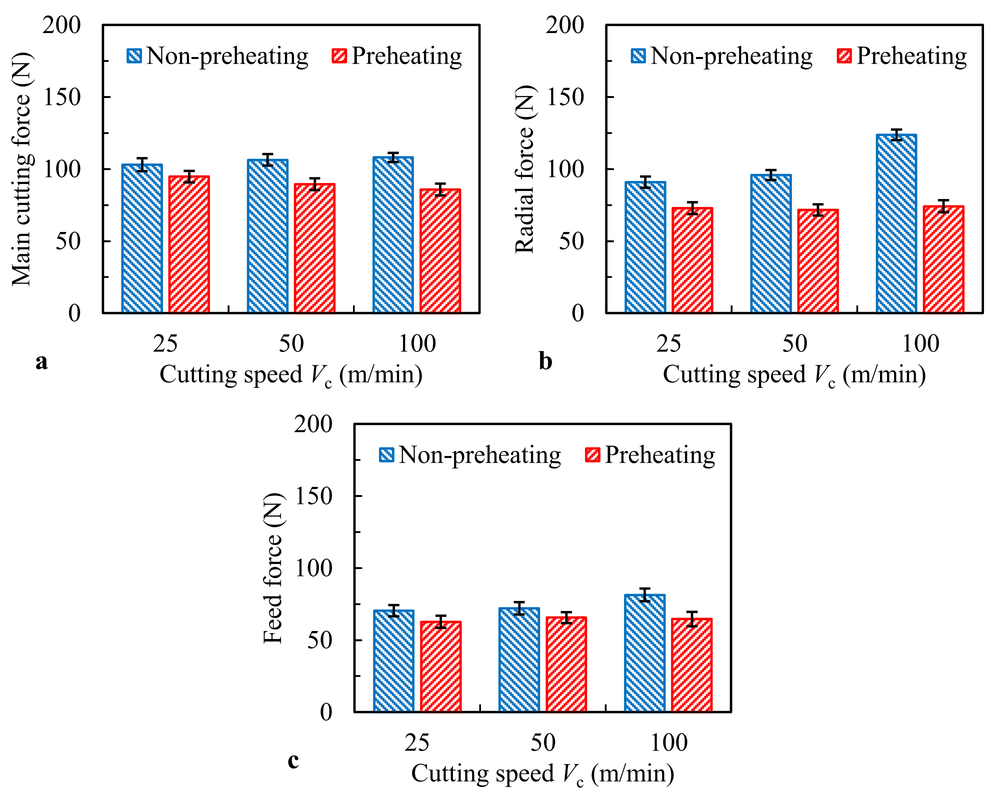

speeds are expected to induce a larger main cutting force in the absence of preheating, owing to the increase in the strength. The critical stress attains its maximum value when the temperature reaches M_d and decreases with a further increase in the temperature [37]. Consequently, the increase in the cutting speed is expected to reduce the main cutting force after the workpiece is preheated to a temperature above the M_d. Moreover, as shown in Fig. 6, increasing the cutting speed during machining under the non-preheating condition increased the super-elastic recovery of the workpiece, thereby increasing the contact area between the flank face of the tool and workpiece. This phenomenon certainly led to an increase in the radial force. As the super-elastic deformation of the workpiece was likely eliminated by the preheating, the decrease in the radial force under the preheating condition could be attributed to the contact area reduction. Consistent with this study, previous studies demonstrated that radial force increases with the increase in the cutting speed in the range of 12.5 to 100 m/min during turning of NiTi alloys under the non-preheating condition [16, 17]. Furthermore, the variation trend of the feed force under different cutting speeds and conditions was similar to that of the radial force, which indicates that the workpiece likely underwent super-elastic recovery along the axial direction. The phenomenon that the feed force increases with the increase in the cutting speed has also been observed in other studies on turning [16, 17] and drilling [11] of NiTi alloys. In practice, the turning process is executed from one end to the other end along the axial direction of the workpiece; thus, the axial recovery likely does not affect the machining accuracy. Previous studies on the preheating-based machining of NiTi alloys have concluded that preheating could not reduce or increase the cutting resistance [16, 17]. As mentioned previously, this phenomenon can be attributed to the fact that the preheating temperature did not reach the M_d.

3.4 Tool wear progression

The tool wear can also represent the effect of the super-elastic recovery of the workpiece on the machining performance of NiTi alloy. Figure 11 shows the progression of the average flank wear VB_a at V_c = 25, 50, and 100 m/min under both the non-preheating and preheating conditions. The initial wear was measured after machining for 1 min, and the remaining wear was measured after machining for 8, 2, and 1 min for V_c = 25, 50, and 100 m/min, respectively. As shown in Fig. 11, the initial wear increased considerably with the increase in the cutting speed under the non-preheating condition. By contrast, under the preheating condition, the initial wear only increased slightly with the increase in the cutting speed, and its value was always smaller than the corresponding value under the non-preheating condition. Table 2 summarizes the tool life at each cutting speed under both the conditions. The tool life

Table 2 Measurement results for tool life

Conditions	Cutting speed V_c (m/min)		
	25	50	100
Tool life (min)			
Non-preheating	80	28	4
Preheating	96	40	8

decreased significantly with the increase in the cutting speed under both the conditions. Compared with that under the non-preheating condition, the tool life under the preheating condition was increased by 20%, 43%, and 100% at V_c = 25, 50, and 100 m/min, respectively. At V_c = 100 m/min, although the tool life under the preheating condition was only 8 min, it was twice as much as that under the non-preheating condition.

Figure 12 shows the tool wear patterns at V_c = 25 m/min under the non-preheating and preheating conditions after machining for 80 min. Because the corner radius of the cutting tool (0.8 mm) was larger than the cutting depth, flank wear occurred on the nose region of the flank face. Under the non-preheating condition, a crater on the rake face, chip adhesion, BUE on the cutting edge, and abrasion marks on the flank face were observed. Because no fracture occurred at the cutting edge and because the distribution of the flank wear was relatively regular, the tool life could be determined considering VB_a. Under the preheating condition, except for the decrease in the flank wear width, the wear patterns were similar. Moreover, similar wear patterns were observed at V_c = 50 m/min.

By contrast, when the cutting speed increased to 100 m/min, a fracture at the cutting edge was observed after machining for 4 min under the non-preheating condition, as shown in Figs. 13a and b. It was inferred that the tool had reached the end of its life at this time owing to the catastrophic tool failure. VB_a could not be measured because the distribution of the flank wear became irregular, as shown in Fig. 13b. Instead, the maximum flank wear VB_{max} was measured. In contrast to the non-preheating condition, no fracture was observed at the cutting edge at V_c = 100 m/min under the preheating condition, as shown in Figs. 13c and d. Moreover, no fracture occurred at the cutting edge even when VB_a exceeded 0.3 mm. Except that no evident crater was observed on the rake face, the tool wear patterns at this cutting speed were similar to those at other cutting speeds.

When machining NiTi alloys using cemented carbide tools, abrasive wear occurs on the flank face [11, 13, 16, 17, 22, 38], crater wear occurs on the rake face [22, 30], and adhesion [22, 30] is generally observed. Accordingly, the tool wear patterns observed in this study are consistent with those in previous studies. However, the severe notch wear reported in other studies [16, 17, 22] was not observed in this study. Weinert

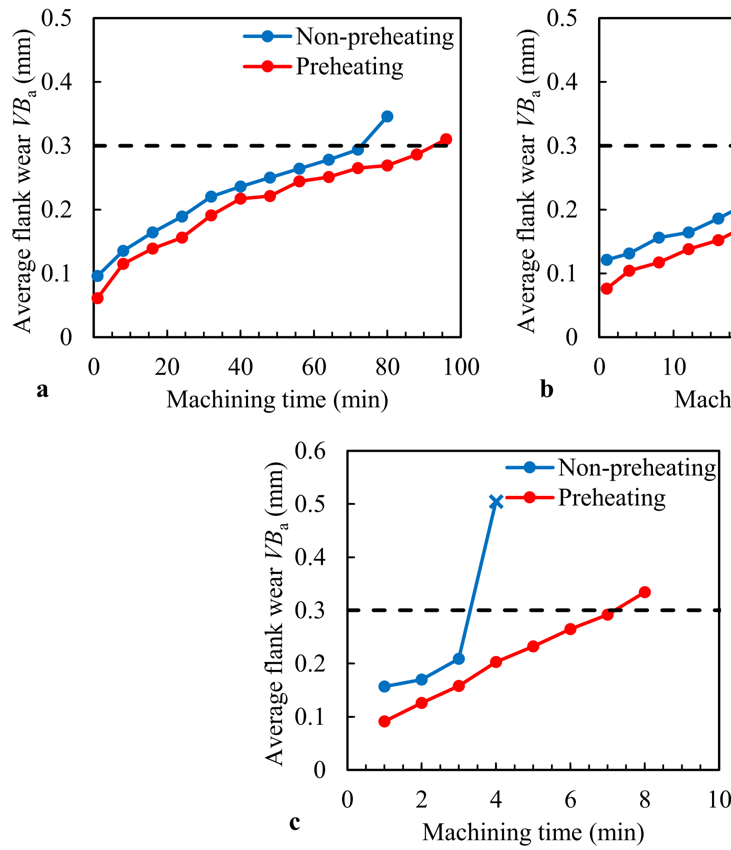

Fig. 11 Progression of average flank wear at V_c = **a** 25 m/min, **b** 50 m/min, and **c** 100 m/min

et al. [11] reported that a lower cutting depth helps reduce the notch wear; hence, the absence of severe notch wear was likely a result of the selection of a relatively low cutting depth in this study (0.5 mm in other studies). The notable increase in the initial wear with the increase in the cutting speed under the non-preheating condition can be attributed to the increase in

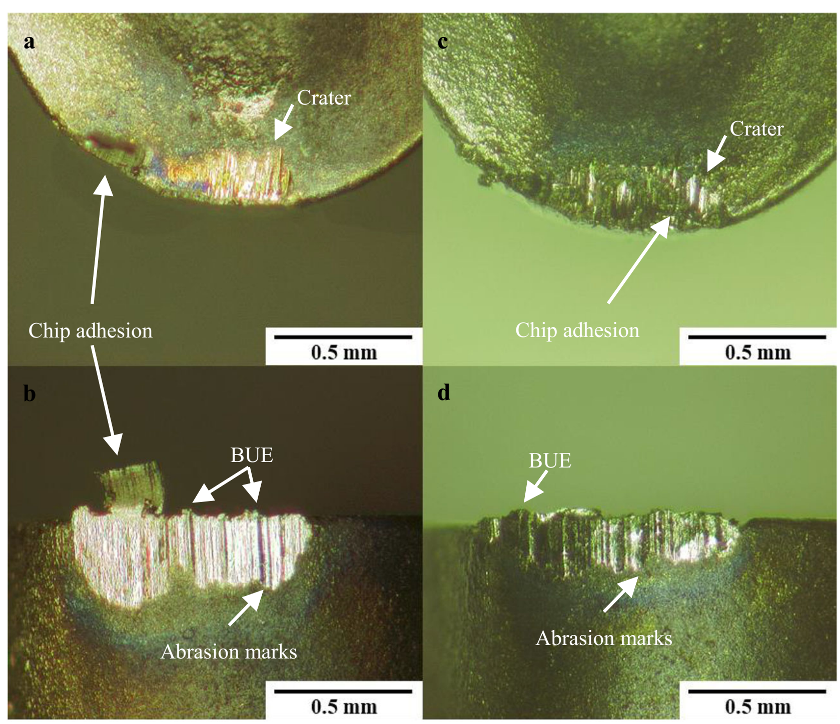

Fig. 12 Tool wear patterns at V_c = 25 m/min after machining for 80 min under **a** and **b** non-preheating condition, **c** and **d** preheating condition

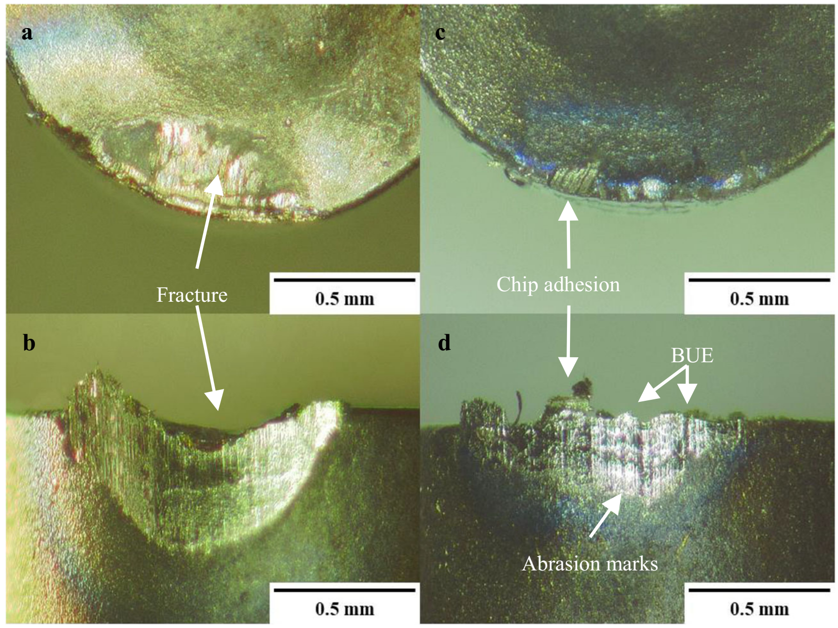

Fig. 13 Tool wear patterns at V_c = 100 m/min after machining for 4 min: **a** and **b** under non-preheating condition, **c** and **d** under preheating condition

the contact area between the flank face of the tool and workpiece, caused by the super-elastic recovery. As mentioned previously, the contact area was reduced owing to the preheating because the super-elastic recovery of the workpiece was eliminated; consequently, the initial wear decreased and increased only slightly with the increase in the cutting speed under the preheating condition. Moreover, the high temperature of the chip (Fig. 5), which was indicative of a high temperature on the tool rake face, together with the high cutting resistance (Fig. 10), resulted in the fracture of the cutting edge at V_c = 100 m/min under the non-preheating condition. Even though the temperature of the chip became higher under the preheating condition than that under the non-preheating condition (Fig. 5), the significant decrease in the cutting resistance under this condition (Fig. 10) protected the tool from fracture. Moreover, the reduction in the crater on the rake face at this cutting speed can be ascribed to the decrease in the contact length between the tool and chip. This decrease in the tool–chip contact length with the increase in the cutting speed has also been observed using a high-speed camera in orthogonal cutting experiments on room-temperature austenitic NiTi alloys [13]. Therefore, the super-elastic recovery of the workpiece reduces the tool life, whereas preheating can prolong the tool life. Besides, a moderate cutting speed in the range of 25 to 50 m/min must be selected to prolong the tool life under both the machining conditions.

4 Conclusion

In this study, the effects of super-elasticity on the machinability of room-temperature austenitic NiTi alloy were investigated, and the cutting condition was optimized by conducting turning experiments at various cutting speeds under non-preheating and preheating conditions. The following conclusions were derived:

(1) During machining under the non-preheating condition, the temperature prerequisite of the phase transformation of the NiTi alloy was satisfied because the temperature of the workpiece did not exceed the M_d.
(2) During machining under the non-preheating condition, owing to the partial reverse phase transformation from martensite to austenite, the workpiece exhibited the super-elastic recovery, which increased with the increase in the cutting speed from 25 to 100 m/min. However, a low cutting speed of 10 m/min is not appropriate for machining NiTi alloys because of the severe BUE deposition on the machined surface.
(3) The super-elastic recovery of the workpiece deteriorated the dimension accuracy, increased the radial force and feed force, and shortened the tool life. Preheating enhanced the dimension accuracy, reduced the radial force and feed force, and prolonged the tool life by eliminating the effect of the super-elastic recovery.
(4) The optimum cutting condition for NiTi alloys is preheating the workpiece to a temperature above the M_d and selecting moderate cutting speeds of 25–50 m/min.

Acknowledgements We gratefully acknowledge the supports received for this study from Furukawa Techno Material Co., Ltd.

Author contribution Not applicable

Funding This research was partially funded by JSPS KAKENHI grant numbers 18K03871 and 16K17997.

Data Availability The datasets used or analyzed during the current study are available from the corresponding author on reasonable request.

Code availability Not applicable

Declarations

Competing interests The authors declare no competing interests.

References

1. Otsuka K, Wayman CM (1999) Shape memory materials. Cambridge University Press, Cambridge
2. Kaya E, Kaya I (2019) A review on machining of NiTi shape memory alloys: the process and post process perspective. Int J Adv Manuf Technol 100:2045–2087. https://doi.org/10.1007/s00170-018-2818-8
3. Benafan O, Moholt MR, Bass M, Mabe JH, Nicholson DE, Calkins FT (2019) Recent advancements in rotary shape memory alloy actuators for aeronautics. Shap Mem Superelasticity 5:415–428. https://doi.org/10.1007/s40830-019-00260-3
4. Xu XJ, Zheng YF (2006) Comparative study of torsional and bending properties for six models of nickel-titanium root canal instruments with different cross-sections. J Endod 32(4):372–375. https://doi.org/10.1016/j.joen.2005.08.012
5. Li XJ, Wang JQ, Han EH, Ke W (2007) Influence of fluoride and chloride on corrosion behavior of NiTi orthodontic wires. Acta Biomater 3(5):807–815. https://doi.org/10.1016/j.actbio.2007.02.002
6. Cheng Y, Cai W, Li HT, Zheng YF (2006) Surface modification of NiTi alloy with tantalum to improve its biocompatibility and radiopacity. J Mater Sci 41:4961–4964. https://doi.org/10.1007/s10853-006-0096-6
7. Mineta T, Mitsui T, Watanabe Y, Kobayashi S, Haga Y, Esashi M (2001) Batch fabricated flat meandering shape memory alloy actuator for active catheter. Sens Actuator A Phys 88(2):112–120. https://doi.org/10.1016/S0924-4247(00)00510-0
8. Weinert K, Petzoldt V, Kötter D, Buschka M (2004) Drilling of NiTi shape memory alloys. Mater Werkst 35(5):338–341. https://doi.org/10.1002/mawe.200400752
9. Wang GJ, Liu ZQ, Huang WM, Wang B, Niu JT (2019) Influence of cutting parameters on surface roughness and strain hardening during milling NiTi shape memory alloy. Int J Adv Manuf Technol 102:2211–2221. https://doi.org/10.1007/s00170-019-03342-9
10. Piquard R, D'Acunto A, Laheurte P, Dudzinski D (2014) Micro-end milling of NiTi biomedical alloys, burr formation and phase transformation. Precis Eng 38(2):356–364. https://doi.org/10.1016/j.precisioneng.2013.11.006
11. Weinert K, Petzoldt V (2004) Machining of NiTi based shape memory alloys. Mater Sci Eng A 378(1):180–184. https://doi.org/10.1016/j.msea.2003.10.344
12. Kong M, Axinte D, Voice W (2011) Challenges in using waterjet machining of NiTi shape memory alloys: an analysis of controlled-depth milling. J Mater Process Technol 211(6):959–971. https://doi.org/10.1016/j.jmatprotec.2010.12.015
13. Shizuka H, Sakai K, Yang H, Sonoda K, Nagare T, Kurebayashi Y, Hayakawa K (2020) Difficult cutting property of NiTi alloy and its mechanism. J Manuf Mater Process 4(4):124. https://doi.org/10.3390/jmmp4040124
14. Kuppuswamy R, Yui A (2017) High-speed micromachining characteristics for the NiTi shape memory alloys. Int J Adv Manuf Technol 93:11–21. https://doi.org/10.1007/s00170-015-7598-9
15. Yang H, Sakai K, Shizuka H, Kurebayashi Y, Hayakawa K, Nagare T (2021) Effect of cutting speed on shape recovery of work material in cutting process of super-elastic NiTi alloy. Int J Automation Technol 15(1):24–33. https://doi.org/10.20965/ijat.2021.p0024
16. Kaynak Y, Karaca HE, Noebe RD, Jawahir I (2015) The effect of active phase of the work material on machining performance of a NiTi shape memory alloy. Metall Mater Trans A 46(6):2625–2636. https://doi.org/10.1007/s11661-015-2828-1
17. Kaynak Y, Karaca HE, Noebe RD, Jawahir IS (2013) Analysis of tool-wear and cutting force components in dry, preheated, and cryogenic machining of NiTi shape memory alloys. Proc CIRP 8:498–503. https://doi.org/10.1016/j.procir.2013.06.140
18. Kaynak Y, Huang B, Karaca H, Jawahir I (2017) Surface characteristics of machined NiTi shape memory alloy: the effects of cryogenic cooling and preheating conditions. J Mater Eng Perform 26(7):3597–3606. https://doi.org/10.1007/s11665-017-2791-7
19. Chen W, Wu Q, Kang JH, Winfree NA (2001) Compressive superelastic behavior of a NiTi shape memory alloy at strain rates of 0.001-750 s−1. Int J Solids Struct 38(50–51):8989–8998. https://doi.org/10.1016/S0020-7683(01)00165-2
20. Motemani Y, Nili-Ahmadabadi M, Tan MJ, Bornapour M, Rayagan S (2009) Effect of cooling rate on the phase transformation behavior and mechanical properties of Ni-rich NiTi shape memory alloy. J Alloys Compd 469(1–2):164–168. https://doi.org/10.1016/j.jallcom.2008.01.153
21. Benafan O, Noebe RD, Padula SA, Garg A, Clausen B, Vogel S, Vaidyanathan R (2013) Temperature dependent deformation of the b2 austenite phase of a NiTi shape memory alloy. Int J Plast 51:103–121. https://doi.org/10.1016/j.ijplas.2013.06.003
22. Kaynak Y, Karaca H, Noebe R, Jawahir I (2013) Tool-wear analysis in cryogenic machining of NiTi shape memory alloys: a comparison of tool-wear performance with dry and MQL machining. Wear 306(1):51–63. https://doi.org/10.1016/j.wear.2013.05.011
23. Zhao YZ, Li JF, Guo K, Sivalingam V, Sun J (2020) Study on chip formation characteristics in turning NiTi shape memory alloys. J Manuf Process 58:787–795. https://doi.org/10.1016/j.jmapro.2020.08.072
24. ISO 3685 (1993) Tool-life testing with single-point turning tools.
25. Frenzel J, George EP, Dlouhy A, Somsen C, Wagner MFX, Eggeler G (2010) Influence of Ni on martensitic phase transformations in NiTi shape memory alloys. Acta Mater 58(9):3444–3458. https://doi.org/10.1016/j.actamat.2010.02.019
26. Vojtech D, Michalcova A (2011) Influence of heat-treatment on mechanical properties and transformation temperatures of nitinol. Key Eng Mater 465:471–474. https://doi.org/10.4028/www.scientific.net/KEM.465.471
27. Kong MC, Lee WB, Cheung CF, To S (2006) A study of materials swelling and recovery in single-point diamond turning of ductile materials. J Mater Process Technol 180(1–3):210–215. https://doi.org/10.1016/j.jmatprotec.2006.06.006
28. Malekian M, Mostofa MG, Park SS, Jun MBG (2012) Modeling of minimum uncut chip thickness in micro machining of aluminum. J Mater Process Technol 212(3):553–559. https://doi.org/10.1016/j.jmatprotec.2011.05.022
29. Yip WS, To S (2017) Reduction of material swelling and recovery of titanium alloys in diamond cutting by magnetic field assistance. J Alloys Compd 722:525–531. https://doi.org/10.1016/j.jallcom.2017.06.167
30. Kaynak Y (2014) Machining and phase transformation response of room-temperature austenitic NiTi shape memory alloy. J Mater Eng Perform 23(9):3354–3360. https://doi.org/10.1007/s11665-014-1058-9

31. Zhao YZ, Guo K, Sivalingam V, Li JF, Sun QD, Zhu ZJ, Sun J (2021) Surface integrity evolution of machined NiTi shape memory alloys after turning process. Adv Manuf. https://doi.org/10.1007/s40436-020-00330-1
32. Otsuka K, Ren X (2005) Physical metallurgy of Ti-Ni-based shape memory alloys. Prog Mater Sci 50(5):511–678. https://doi.org/10.1016/j.pmatsci.2004.10.001
33. Kaynak Y, Karaca H, Jawahir I (2015) Cutting speed dependent microstructure and transformation behavior of NiTi alloy in dry and cryogenic machining. J Mater Eng Perform 24(1):452–460. https://doi.org/10.1007/s11665-014-1247-6
34. Mitwally ME, Farag M (2009) Effect of cold work and annealing on the structure and characteristics of NiTi alloy. Mater Sci Eng A 519(1–2):155–166. https://doi.org/10.1016/j.msea.2009.04.057
35. Li Y, Li JY, Liu M, Ren YY, Chen F, Yao GC, Mei QS (2015) Evolution of microstructure and property of NiTi alloy induced by cold rolling. J Alloys Compd 653:156–161. https://doi.org/10.1016/j.jallcom.2015.09.056
36. Nemat-Nasser S, Guo WG (2006) Superelastic and cyclic response of NiTi SMA at various strain rates and temperatures. Mech Mater 38(5–6):463–474. https://doi.org/10.1016/j.mechmat.2005.07.004
37. Adharapurapu RR, Jiang FC, Vecchio KS, Gray ШGT (2006) Response of NiTi shape memory alloy at high strain rate: a systematic investigation of temperature effects on tension–compression asymmetry. Acta Mater 54(17):4609–4620. https://doi.org/10.1016/j.actamat.2006.05.047
38. Guo Y, Klink A, Fu C, Snyder J (2013) Machinability and surface integrity of nitinol shapememory alloy. CIRP Ann Manuf Technol 62(1):83–86. https://doi.org/10.1016/j.cirp.2013.03.004